

Physicochemical Properties and Possible Applications of Waste Corncob Fly Ash from Biomass Gasification Industries of China

Xiwen Yao, Kaili Xu,* and Yang Li

As a by-product generated from the processing of corn, the production in China of corncob (CC) is abundant, with up to 3.87 million tons per year. The biomass gasification industries make use of the CC residue as feedstock, but large volumes of generated corncob ash (CCA) requires daily disposal. In this study, CCA was characterized by laser particle size analyzer (LPSA), X-ray fluorescence (XRF), X-ray diffraction (XRD), thermal gravimetric and differential thermal analysis (TG-DTA), scanning electron microscopy, and energy dispersive X-ray (SEM-EDX). XRF results showed that the CCA was rich in K, Ca, and P, indicating its potential as a soil amendment. High content of SiO₂ in CCA revealed its potential as a pozzolan in blended cement concrete. XRD showed the presence of crystal phases such as potassium carbonate, sylvite, arcanite, quartz, calcite, and nitrite. SEM images revealed the high agglomeration of CCA. EDX gave evidence of the external surface of agglomerated particles coated with KCl. TG-DTA analysis indicates that decomposition of CCA has stepwise mechanism. The CCA powders through a 0.154 mm sieve showed a high specific surface area of 162.32 m²/g, average pore size of 12.17 Å with pore volume of 0.116 cm³/g. The carbon residue separated from CCA has the potential to be used as activated carbon.

Keywords: Biomass; Corncob ash; Gasification; Ash characteristics; Applications

Contact information: School of Resources and Civil Engineering, Northeastern University, Shenyang 110819, China; *Corresponding authors: kaili_xu@aliyun.com

INTRODUCTION

In the past decades, there has been a growing interest in the exploration of “green” renewable energy sources due to the increasing fuel demand and the shortcomings of existing fossil fuel energy sources such as greenhouse gas emissions and other harmful effects on the environment (McKendry 2002; Umamaheswaran and Batra 2008; Du *et al.* 2014). Globally, biomass resources regarded as a green renewable energy have potential for being important feedstock fuels for the future energy production. This possibility has attracted worldwide attention regarding their renewable nature, carbon dioxide-neutral characteristics, and world-wide availability (Haykiri-Acma *et al.* 2013). Consequently, many countries are placing great emphasis on the exploration of bioenergy, and the techniques used are various, such as combustion, gasification, pyrolysis, and hydrogen production (Wang *et al.* 2008).

Corn is an important cereal crop that is extensively harvested throughout the world. In China alone, the yield of corn reached 2.15×10⁸ tons in 2014 according to China Statistical Yearbook from the China's National Bureau of Statistics. Since the ratio between corn grain and corncob (CC) is approximately 100:18 (Cao *et al.* 2004), it can be

estimated that the quantity of corncob generated in China every year is about 3.87×10^7 tons. Usually, cornstalk (CS) is retained on the farmlands by corn harvesters for the purpose of using it in soil as a fertilizer to improve productivity and fertility of soil. By contrast, the CC may be collected, transported, and separated together with the corn grain, and serve as a raw material in making low-grade fuels in many parts of the world (Liu *et al.* 2014), which causes a lot of waste of the CC resources. Hence, it is necessary to take a proper processing method to utilize the CC to produce economically viable products. Converting biomass *via* thermochemical conversion technology to produce high quality products has become more and more popular in recent years. Many studies are focusing on gas and liquid products that are produced from biomass residues through pyrolysis. These products are potential renewable energy sources, and the typical products are CO₂, CO, H₂O, CH₄, NH₃, acids (*e.g.* CH₃COOH), and aldehydes (*e.g.* furaldehyde) (Cao *et al.* 2004). Among different bioenergy conversion methods determined by the demand and supply of available types and quantities of feedstock, combustion and gasification are the most popular processing technologies (McKendry 2002).

In China, the biomass gasification industries mainly consist of biomass power generation and biomass gasification central gas plants. There exist today more than 600 biomass gasification plants that are routinely operating and potentially producing biomass gas for more than 2.096×10^5 households (Zhou *et al.* 2014). This production plays an important role not only in dealing with environmental pollution problems caused by direct combustion of agricultural waste, but also in efficient utilization of the residual biomass resources in rural areas. It is, nevertheless, problematic that the inorganic mineral substances left after the thermochemical conversion are ashes containing various forms of alkali and alkali earth metals and considerable amount of silica (Wang *et al.* 2008; Du *et al.* 2014). As a result, the biomass ash is easy to melt and volatilize (Arvelakis *et al.* 2004; Thy *et al.* 2006). These characteristics usually result in fouling, slagging, and corrosion during the gasification process (Jensen *et al.* 2000; Knudsen *et al.* 2004; Kilpimaa *et al.* 2013).

A number of studies have characterized biomass ash (Jensen *et al.* 2000; Arvelakis *et al.* 2004; Knudsen *et al.* 2004; Thy *et al.* 2006; Wang *et al.* 2008; Niu *et al.* 2010; Abraham *et al.* 2013; Wang *et al.* 2013; Du *et al.* 2014). There are also many studies focused on the utilization of biomass ash in various fields, for example, as a raw material for ceramic products (Abraham *et al.* 2013), as an adsorbent (Vassilev *et al.* 2013; Maneerung *et al.* 2016), as a potential source of SiO₂ (Terzioglu and Yucel 2012; Terzioglu *et al.* 2013), as a construction and building material (Adesanya and Raheem 2010), as a soil amendment (Umamaheswaran and Batra 2008; Pan and Eberhardt 2011), and as a source for potash production (Ogundiran *et al.* 2011). However, research on the physicochemical properties of CCA obtained from biomass gasification plants is limited, and its physicochemical behavior remains uncertain. Because of this, the potential applications of CCA from biomass gasification plant remains unexplored. The present study therefore focuses on the preliminary properties of waste CCA to provide a basis for analyzing how to transform the waste CCA into ecofriendly and value added products (such as adsorbent, raw material for ceramic products, cement and concrete additive, soil amendment, and material recovery). For this purpose, analytical techniques such as X-ray fluorescence spectroscopy (XRF), X-ray diffraction (XRD), thermal gravimetric and differential thermal analysis (TG-DTA), and scanning electron microscopy (SEM), coupled with energy dispersive X-ray (EDX) have been applied to obtain information on

the chemical constituents, mineral phases, thermal behavior, micromorphology, and surface composition of CCA. Besides, particle size analyzer (based on laser diffraction) was used to determine the particle size distribution.

EXPERIMENTAL

Description of the Gasification Plant

The biomass gasification plant (located in the peripheral rural area of Shenyang, Liaoning province, China) has a maximum thermal input of 175 kW, which can provide biomass gas for about 300 households by using CC waste as feedstock simultaneously. The whole plant covers an area of 58 m². The gasifier is a downdraft fixed bed type, which has an internal diameter of 1.03 m and a height (from the gasifier top to the grate) of 1.88 m. The gasification starts with preheating of the bed by means of an external burner. Once the gasifier is heated up to about 200 °C (temperature at the combustion zone in the inner wall of gasifier), air will enter the gasifier with an equivalent ratio of 0.8. The biomass gas was mainly generated between 680 and 850 °C. This gasification plant is equipped with a gas purification system consisting of three basic components: a cyclone dust collector, a spray-dryer system, and a tar scrubber.

Materials

General characterization of CC and CCA

The CC samples used in this study (from rural area of Shenyang) are common in northern China. Before the experiments, the samples were dried, ground using a high speed rotary cutting mill and then pulverized and grinded to a particle size of < 0.154 mm.

The CCA samples were collected from the cyclone dust collector of biomass gasification plant. The raw ash samples were firstly pulverized using a ball mill to make them symmetrical for the sake of their asymmetrical features. Secondly, they were placed into a pan and then an oven to be dried at 105 °C ± 0.5 °C for 24 h. However, after the samples were dried and cooled, they might be bonding together again. So, they were ground again to be homogenized. Finally, the ash samples which passed through a 0.154 mm sieve were collected in a closed vessel and retained to be analyzed.

The volatile matter (VM), fixed carbon (FC), and ash content (A) in the received CC and CCA samples were measured by 5E-MACIII Infrared Speediness Coal Analyzer of Kaiyuan Apparatus Company, China. The moisture (M) was determined by Sartorius Moisture Analyzer IMA 30. Ultimate analysis was analyzed quantitatively by Vario MACRO Elemental Analyzer of Elementar, Germany. The low heating value (LHV) of the CC samples was measured by IKA Calorimeter System C2000. Table 1 lists the general characterization of CC and CCA. All values presented a good reproducibility with the standard deviation of < 2.0%, and the precision of the measurements was 0.5%.

Table 1. General Characterization of CC and CCA

Samples	Proximate analysis (wt.%)				Ultimate analysis (wt.%)					LHV (kJ/kg)
	M _{ad}	A _{ad}	VM _{ad}	FC _{ad}	C _{ad}	H _{ad}	O _{ad}	N _{ad}	S _{ad}	
CC	0.87	2.24	79.25	17.64	47.26	5.79	43.23	0.56	0.05	18150
CCA	0.78	8.62	3.87	86.73	78.49	1.24	10.36	0.45	0.06	-

Notes: ad, air dried basis. All values are on an air dried basis.

Experimental Apparatus

The experimental methods and procedures for characteristic analysis on ash were:

(a) Particle size distribution was analyzed by laser particle size analyzer (LPSA) (Winner 3001, Jinan Micro-nano Particle Instrument Co. Ltd., Shandong province, China) equipped with the He-Ne laser diffraction ($\lambda = 632.8$ nm),

(b) Elemental composition of the ash was measured by X-ray fluorescence spectrometer (XRF) (ZSX100e, Rigaku Co. Ltd, Japan). Each test used about 2 g samples. As for the XRF analysis, the major elements (presented in concentrations more than 10,000 $\mu\text{g/g}$) happened to be Si, K, S, Cl, Ca, and Mg. Minor constituents (1000 to 10,000 $\mu\text{g/g}$) included Al, Fe, and Na. Other elements (less than 1000 $\mu\text{g/g}$) included Ti and Mn, which were also given in the XRF analysis. Repeated experiments were carried out three times and the average value was used to minimize the error,

(c) Crystalline compounds in ash were identified by X-ray diffractometer (XRD) (X'Pert PRO, PANalytical B.V., The Netherlands) with Cu K α radiation ($\lambda = 0.15406$ nm) at a scan rate of 0.02° per second. The operation voltage and current were maintained at 36 kV and 50 mA, respectively. Data were collected from 5° to 80° on a 2θ scale. Peak identification was performed through comparison with standards coming from High Score Plus software package,

(d) Surface morphology was observed by scanning electron microscopy (SEM) (Ultra Plus, Carl Zeiss Co. Ltd., Germany) with an accelerating voltage of 20 to 30 kV. The micrographs at different magnifications were generated by a computer program. Surface composition was analyzed by energy dispersive X-ray (EDX) (Genesis, Edax DX-4) at an accelerating voltage of 25 kV. The EDX analysis was performed in a spot mode in which the beam was localized on a single area manually chosen within the field of view. The location was shown on the provided micrographs by a "+". The EDX detector was set up for detecting elements with atomic number equal to or greater than six,

(e) Thermal analyses were carried out using a thermogravimetric analyzer (TGA) (NETZCH-STA449 F3, Germany) to obtain the weight loss, as well as the differential thermal behavior (DTA) to obtain information on phase transitions. The sensitivity was 1 μg and 0.01 °C. Each test used about 5 mg samples. The temperature range was from 30 to 1200 °C at a heating rate of 20 °C/min. The heating was carried out in nitrogen, dry air, and 40% O₂ in N₂, respectively. The flow rate of carrier gas was 30 mL/min.

RESULTS and DISCUSSION

Chemical Analysis

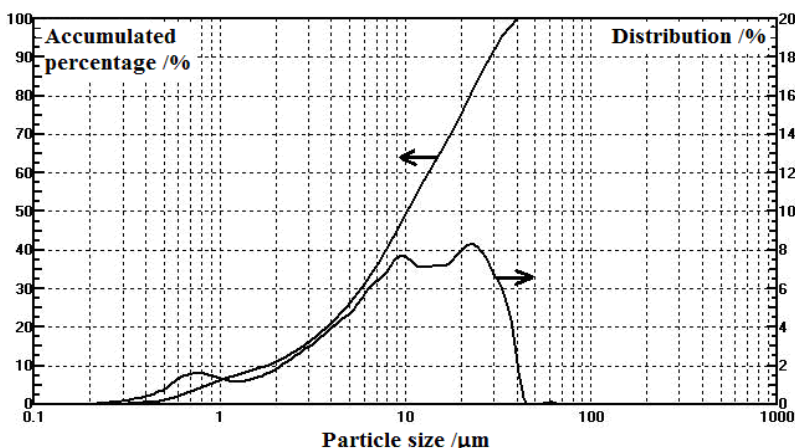
In this study, all elements obtained by XRF analysis were translated into oxides (Cl converted to equivalent oxygen), and then normalized. The composition expressed as oxides (except Cl) is listed in Table 2. From the results, one can find that the CCA samples were mainly composed of SiO₂, K₂O, CaO, P₂O₅, and Cl. Moreover, K₂O and SiO₂ were predominant in the composition. This was also confirmed by XRD data, which displayed the presence of potassium in the forms of arcanite, kaliginite, kalsilite, leucite, sylvite, as well as silica in the form of quartz as the major component. Besides, the other compounds such as Na₂O, MgO, SO₃, Fe₂O₃, Al₂O₃, TiO₂, and MnO were also present.

Table 2. Elemental Composition of CCA Determined by XRF Analysis (wt.%)

SiO ₂	K ₂ O	Na ₂ O	CaO	MgO	SO ₃	Fe ₂ O ₃	Al ₂ O ₃	TiO ₂	MnO	P ₂ O ₅	Cl
28.39	31.50	4.99	9.72	1.66	2.52	1.10	3.58	0.21	0.09	7.53	8.71

Particle Size Distribution

The particle size distribution of the CCA powders selected by a 0.154 mm sieve is shown in Fig. 1. The results of granularity analysis are listed in Table 3. Repeated tests were carried out three times, and the average value was used to minimize the error. The mean diameter and the medium diameter of the sieved powders were 12.96 μm and 10.23 μm , respectively. The accumulated percentage for the ash particles within diameter of 30 μm occupied more than 90%. Furthermore, the value of the S/V for these sieved powders was rather large, 14626.5 cm^2/cm^3 . The precision of the measurements was 1.0%, and the results presented a good reproducibility with the standard deviation of < 3.0%.

**Fig. 1.** Particle size distribution of CCA powders**Table 3.** The Granularity Analysis Results of CCA Powders

D_{10} (μm)	D_{25} (μm)	D_{50} (μm)	D_{75} (μm)	D_{av} (μm)	S/V (cm^2/cm^3)
1.76	4.62	10.23	19.40	12.96	14626.5

Notes: D_{10} stands for ash particle diameter, below which the accumulated percentage is 10%; D_{25} stands for particle diameter, below which the accumulated percentage is 25%, etc; D_{av} stands for the mean diameter; S/V stands for the ratio of the total surface area and volume of the particles.

Phase Composition

Figure 2 illustrates the result of XRD analysis, indicating the qualitative presence of crystalline minerals. It can be seen from the figure that the CCA mainly were composed of a mixture of potassic compounds such as potassium bicarbonate (KHCO_3), potassium aluminum silicate (KAlSiO_4 and KAlSi_2O_6), sylvite (KCl), and arcanite (K_2SO_4). Furthermore, silica was in addition present in the form of low quartz, and calcium and sodium were respectively present in the form of calcite (CaCO_3) and natrite (Na_2CO_3). Besides, it was identified by XRD analysis that potassium present in the form of sylvite was the major crystalline phase. But other forms of potassium (potassium bicarbonate, potassium aluminum silicate, and arcanite) were not detected much. The potassium hydroxide was not detected at all.

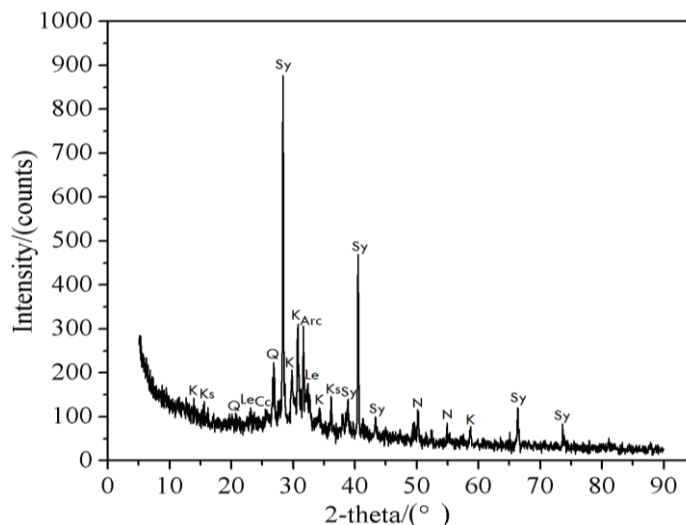


Fig. 2. XRD pattern of CCA powders. Abbreviations: Arc, arcanite (K_2SO_4); Cc, calcite ($CaCO_3$); K, kalicinite ($KHCO_3$); Ks, kalsilite ($KAlSiO_4$); Le, leucite ($KAlSi_2O_6$); Q, quartz (SiO_2); Sy, sylvite (KCl); N, natrite (Na_2CO_3)

From Fig. 2 it is easy to observe that these CCA powders had just one highly crystalline structure with potassium in the form of sylvite. Similar compounds of the CCA have been reported in the literature (Vassilev *et al.* 2013). In addition, these CCA powders also had some amorphous lumps, as can be seen from the broad peak between 10° and 25° in Fig. 2. According to Vassilev *et al.* (2013), these amorphous lumps are probably due to the very fine crystalline mixture without a well defined structure.

SEM-EDX Analysis

In this study, a metal spraying treatment (gold/carbon coating for the sake of conductivity) prior to SEM-EDX analysis was necessary since the electric conductive performance of CCA is poor. After the metal spraying treatment, the SEM-EDX was employed to provide detailed imaging information as well as the surface composition of these ash samples. Figure 3 shows SEM images at different magnifications. As can be seen from Fig. 3, the CCA powders were agglomerated and irregular in shape. The majority of these particles ranged in size from 1 to $100\ \mu m$ (Fig. 3A), which can be sorted into three groups – lacelike (Fig. 3B), quadrate (Fig. 3C), and agglomerate particles (Fig. 3D). Spectra of EDX analyses in points a-c in Fig. 3 are shown in Fig. 4. Although the peak intensity in EDX analysis is not a quantitative measure of elemental concentration, relative amounts can also be inferred from relative peak heights. The precision of EDX analyses was 1.0%, and the coefficient of variation for each spot analysis was $< 0.5\%$.

As can be seen from Fig. 3C, there were some quadrate crystal phases. The EDX analysis in point a (Fig. 4a) illustrates that the major constituents for the quadrate particles were Si and O. This result is consistent with XRD analysis (Fig. 2) which reveals that silica was present in the form of low quartz. Park *et al.* (2003) suggested that SiO_2 is basically in the amorphous state under $800\ ^\circ C$, and only when the temperature exceeds $900\ ^\circ C$, those SiO_2 entities having microcrystalline structure can become transformed into crystalline form from the amorphous state. In the received CCA, the crystal phases were mostly formed at above $900\ ^\circ C$ during gasification process, so the quadrate crystal phases are inferred to be quartz.

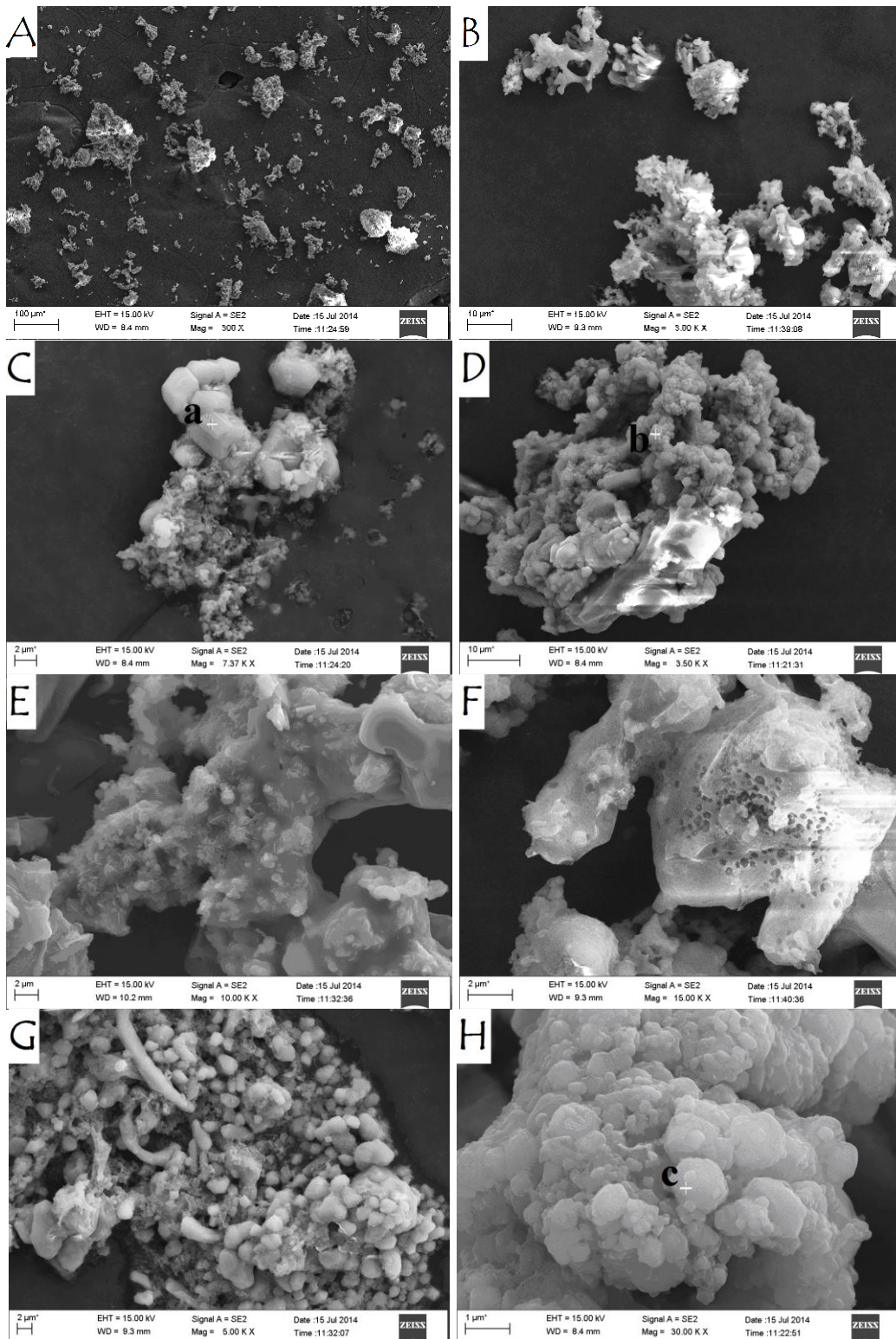


Fig. 3. SEM images at different magnifications of the overall morphology of the ash (A), lacelike particles (B), quadrate particles (C), the external surface of a typical agglomerate sample (D), details of a fused zone suggesting the start of ash softening or surface melting (E), details of the interior of a piece of another agglomerate sample that was broken (F), a significant amount of agglomerated particles bonding together (G), and details of selected zones of the external surface of the agglomerated particles at higher magnification (H)

Figure 3D shows a typical agglomerate sample larger than 50 μm in size at 3500-fold magnification. During the gasification process, small particles tend to be aggregated into larger aggregates. At a closer examination of Fig. 3D, large voids can be found throughout the agglomerate. Results of EDX analysis in point b (Fig. 4b) show that the major elements on the surface of agglomerate samples were Si, O, K, Mg, Ca, P, and S in various compounds; lesser amounts of the elements C, Na, Al, and Cl were also observed.

As can be seen from Fig. 3E, extensive melting on the external surface of ash is evident, indicating the ash surface to be a layer of solidified molten material. Many zones appear to be fused and re-solidified. Within the fused material, however, partially molten or non-molten ash inclusions are clearly visible. According to Zhang *et al.* (2015), the formation of potassium silicate could offer a low melting point around 900 $^{\circ}\text{C}$, which would lead to a strong corrosion under gasification conditions.

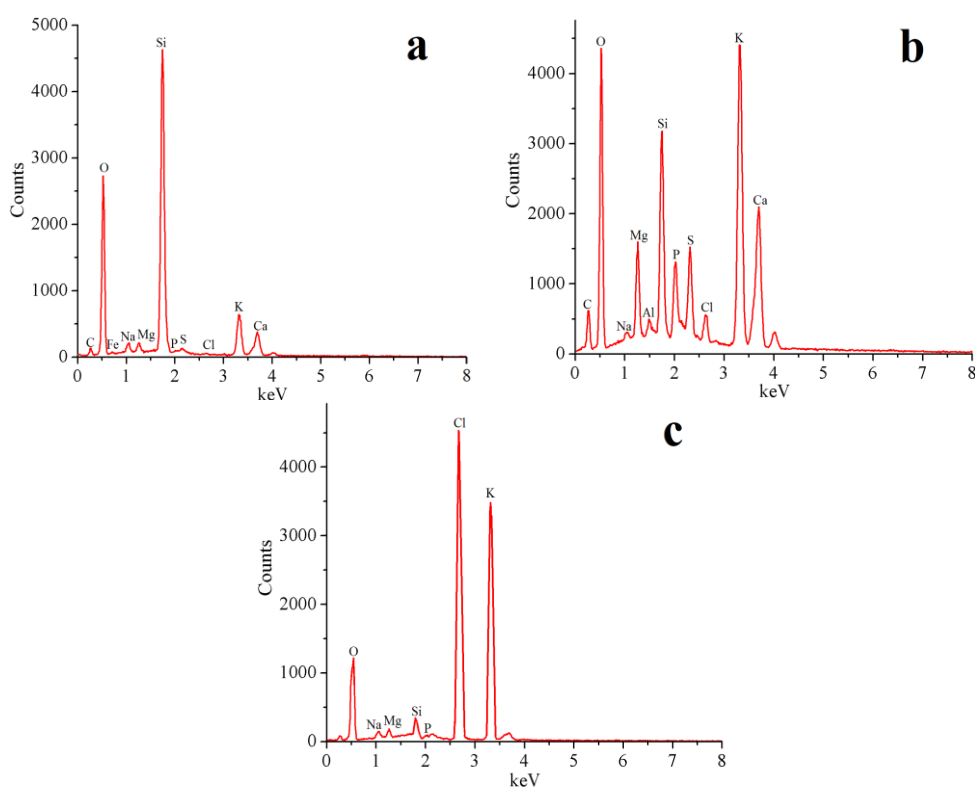


Fig. 4. Spectra of EDX spot analyses in points a-c in Fig. 3

Figure 3F shows selected zones of the internal surface of another agglomerate that was broken before observation. After an inspection of the broken agglomerate, one can clearly identify a porous structure with many pores on its internal surface, indicating the release of some volatiles from the solid substrates during gasification of biomass.

Figures 3G and H show the SEM images of agglomerated particles bonding together, and selected zones of these agglomerated particles at higher magnification. At a closer observation of Fig. 3H, a significant amount of nearly spherical particles (light grey) appear to be tightly connected to each other by sticky points. Results of EDX spot analysis of selected zones of the agglomerated particles (Fig. 4c) illustrate that the predominant elements on the surface of agglomerated particles were K and Cl, indicating that the external surface of these agglomerated particles was mainly coated with KCl.

Thermal Properties Analysis

Thermogravimetric analysis of CC

In order to better understand the pyrolysis characteristics of the raw feedstock, the thermogram curves of CC heated at 20 °C/min under nitrogen are shown in Fig. 5.

As seen from the TG curve in Fig. 5, the decomposition of CC had stepwise mechanisms. The first weight loss (below 140 °C) started at about 70 °C due to loss of moisture from the samples, then followed a major weight loss (within 140 to 420 °C) due to the thermal degradation of biomass. Finally, there was no significant weight loss above 420 °C, and the pyrolytic process was almost complete at approximately 600 °C.

As can be seen from the DTG curve in Fig. 5, initially the degradation rates were slow. However, there was a distinct shoulder peak within 70 to 140 °C. Simultaneously, as can be seen from the DTA curve, there was an endothermic peak at around 100 °C, indicating the energy adsorbed during the volatilization of moisture from the samples.

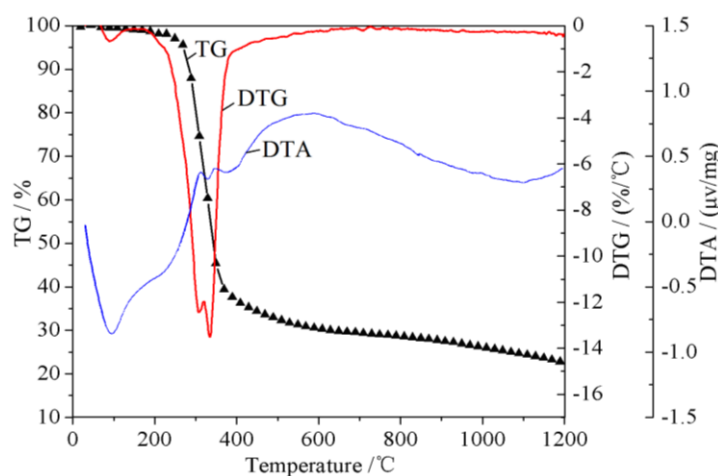


Fig. 5. Thermogram curves of CC feedstock heated at 20 °C/min under nitrogen

When the temperature was above 140 °C, a rapid degradation of CC feedstock was evident. The weight loss between 140 and 420 °C is mainly attributed to evolution of the volatiles from biomass pyrolysis. The weight loss within 140 to 410 °C contributes to most of the weight loss (around 80 to 90 wt.%). Furthermore, as can be seen from the DTG curve in Fig. 5, there exist two sharp weight loss rate peaks respectively at 308 °C and 334 °C in this active pyrolysis zone (between 140 and 420 °C).

At temperatures above 420 °C, an insignificant weight loss was found at a very slow degradation rate. Based on the TG curve in Fig. 5, during the whole pyrolytic process, the residual char yield can be determined as 22.8 wt.%. Hence, the total weight loss of the CC samples was around 77.2 wt.% based on the original biomass weight.

Thermogravimetric analysis of CCA

In this section, effects of pyrolysis atmospheres on the thermal properties of CCA powders were investigated. Figures 6a-c shows the TG-DTA-DTG thermograms under three different atmospheres to represent carbonization under nitrogen and burning under dry air or under 40% O₂ in N₂. The intense internal reactions that occur within ash can be predicted through a comprehensive analysis of TG-DTA-DTG curves. The weight loss as a function of temperature recorded in nitrogen and dry air is respectively shown in Figs. 6a and b. These results, in general show a total weight loss of 17.13 wt.% under nitrogen

and that of 19.86 wt.% under dry air when the ash was heating up to 1200 °C. But the maximum weight loss was in the case of 40% O₂ in N₂, which lost up to 23.12 wt.%.

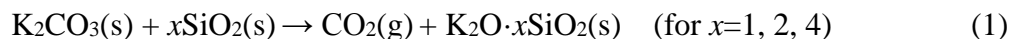
The decomposition under inert or oxidative atmosphere is a complex process, which involves a series of consecutive reactions. As can be seen from Figs. 6a-c, the decomposition had stepwise mechanisms and mainly occurred in four steps that can be explained from the chemical composition of the ash.

The first stage lay below 250 °C, in which the initial weight loss was mainly associated with degradation of thermally unstable organic constituents, which mostly include hemicellulose and lignin (Vassilev *et al.* 2013; Yang *et al.* 2007).

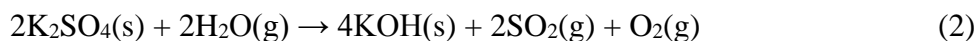
In the second stage, between 250 and 600 °C, the weight loss with heating was continuous, while the reaction rate becomes relatively slow. Under oxidative atmosphere, the combustion of residual organic matter was mainly triggered within 250 to 600 °C.

The third stage was from 600 to 800 °C, in which the weight loss is related to the release of KCl and the release of CO₂ from the thermal decomposition of CaCO₃.

The last stage took place beyond 800 °C and continued until the final temperature. The weight loss of this stage was caused by thermal transformation and volatilization of the residual inorganics. A small weight loss rate peak appeared at temperatures of 850 to 1150 °C (Fig. 6d), indicating a reaction between silica and potassium that appears as a potassium silicate from the reaction of K₂CO₃ with SiO₂. Hence, this weight loss rate peak between 850 and 1150 °C was partially due to CO₂ release when K₂CO₃ reacts with SiO₂. SiO₂ can react with K₂CO₃ according to reaction 1 (Tortosa Masiá *et al.* 2007):



Furthermore, after investigating the thermal properties of wheat straw ash from combustion, Du *et al.* (2014) suggested that the weight loss above 1000 °C might be attributed to the decomposition of relatively stable K-bearing species such as K₂SO₄. Besides, K₂SO₄ can react with H₂O according to reaction 2 (Knudsen *et al.* 2004). As some arcanite (K₂SO₄) was present in the samples (Fig. 2), the release of SO₂ and O₂ from the reaction of K₂SO₄ with H₂O should also be considered for the contribution to the small weight loss rate peak within 850 to 1150 °C.



Above 1150 °C and up to 1200 °C, the weight loss may be caused by the gas-phase release of a minor amount of potassium. Moreover, the decomposition of some silicates, such as the decomposition of K₂SiO₄ (Knudsen *et al.* 2004) and Ca₂SiO₄ (Thy *et al.* 2006) within 1150 to 1200 °C, can also contribute to the weight loss of this high temperature zone. As can be seen from Fig. 6d, with increasing oxygen concentration in the pyrolysis atmosphere, the weight loss rate below around 250 °C increased, indicating that the presence of oxygen under oxidative atmosphere accelerated the pyrolysis process significantly. By contrast, it can be clearly seen from Fig. 6d that the temperature of the maximum weight loss rate decreased with the increase of oxygen concentration.

As revealed by XRD analysis, the CCA contained a great amount of KCl. In the case of nitrogen (Fig. 6a), the small endothermic peak near 620 °C may be due to the melting of KCl. The endothermic region in the DTA curve within the range 600 to 650 °C also indicates that the inorganics need energy for their transformations. By contrast, under oxidative atmosphere, a slight exothermic peak around 630 °C can be clearly seen

in Figs. 6b and c, indicating that the pyrolytic process within 600 to 650 °C shifted from slightly endothermic to exothermic. In fact, although the biomass was being burnt under sufficiently high temperature in the gasifier, there is always some inefficiency on carbon conversion due to kinetic and mass transfer limitations (Rajamma *et al.* 2009). Hence, this transition within 600 to 650 °C was due to the combustion and volatilization of carbon residue generated from inadequate conversion of biomass during gasification process.

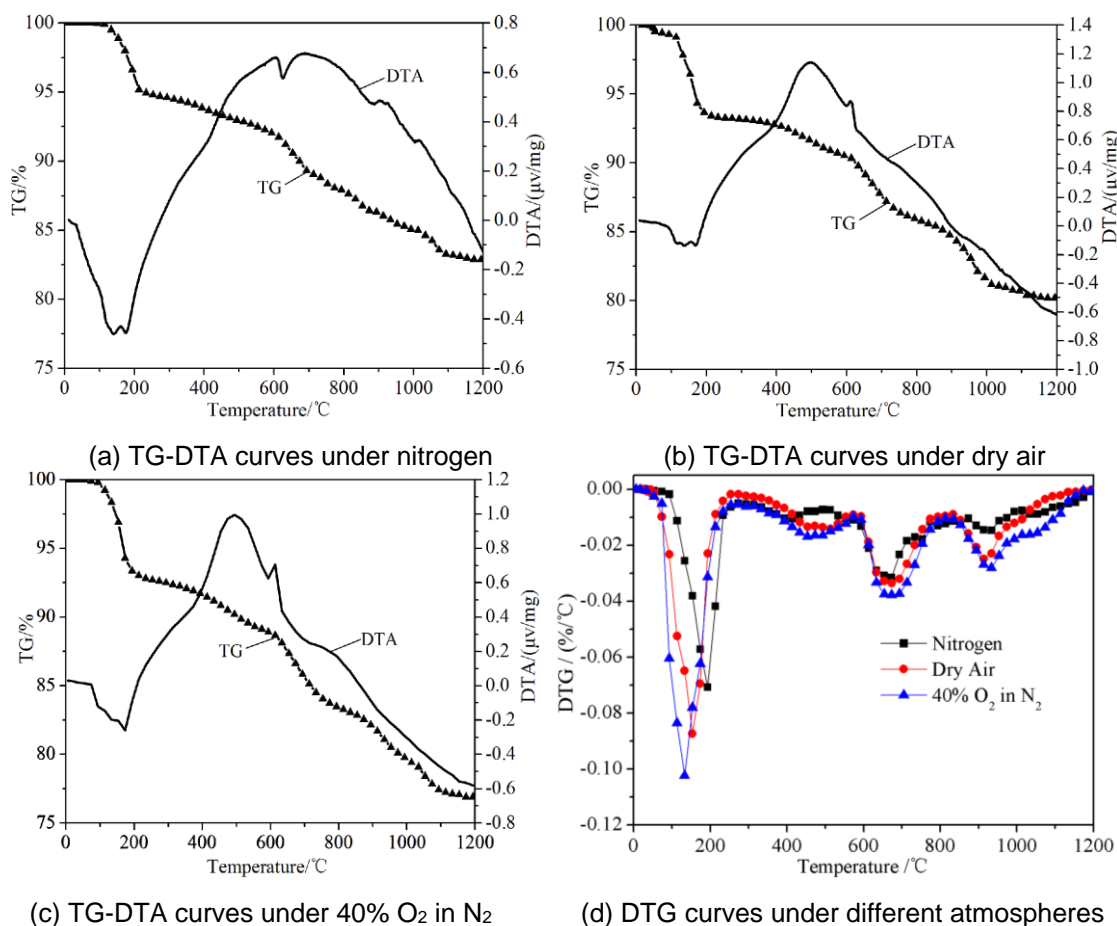


Fig. 6. TG-DTA-DTG thermograms of CCA powders under three different atmospheres

In the case of a nitrogen atmosphere, the weight loss between 400 and 600 °C was about 1.83 wt.%. In the case of dry air and 40% O₂ in N₂, the weight loss between 400 and 600 °C reached up to 2.28 wt.% and 4.46 wt.%, respectively, accompanied by a broad exothermic peak due to volatilisation of the carbon residue. Besides, part of weight loss occurring beyond 700 °C is probably caused by the volatilization of alkali-containing compounds, and this result is in good agreement with Umamaheswaran and Batra (2008), who demonstrated that the remaining weight loss occurring beyond 700 °C could be due to KCl volatilization in the thermal analysis of groundnut ash.

Pore Properties Analysis

In this section, the pore properties of the received CCA were investigated. The important pore properties vital for CCA as an adsorbent in terms of carbon content, specific surface area, pore size, and pore volume were all measured. As can be seen from

the ultimate analysis in Table 1, the carbon content was determined to be as high as 78.49 wt.%. The specific surface area, pore volume, and pore size were determined by nitrogen adsorption measurement using a Quantachrome Autosorb-6B analyzer. The ash samples were firstly degassed for 12 hours under vacuum at 200 °C prior to analysis to remove any adsorbed species. Then the analysis was carried out with nitrogen as adsorbate. Results of these pore properties of CCA are summarized in Table 4.

Table 4. Pore Texture Parameters and Carbon Content of the Received CCA

Carbon content (wt.%)	Specific surface area (m ² /g)	Pore size (Å)	Pore volume (cm ³ /g)
78.49	162.32	12.17	0.116

As presented in Table 4, the received CCA samples exhibited a high specific surface area of 162.32 m²/g, and an average pore size of 12.17 Å with a pore volume of 0.116 cm³/g, indicating that these pore properties vital for CCA as an adsorbent were similar to those of activated carbon (Maneerung *et al.* 2016). As a result, the carbon content of CCA was high, which indicates, together with high porosity, that the carbon residue separated from CCA can potentially be utilized as a source for producing activated carbon. Thus considering the increasing demand for cheap sources of adsorbents, these pore properties make CCA possible as a low cost precursor for the production of adsorbents.

Potential Applications of CCA

As determined by XRF analysis, the CCA from gasification had high contents of Si, K, and Ca, which are very beneficial for the production of dense bodies used in the traditional ceramic industries. The CCA shows potential utilization for ceramic products such as structural ceramics and membrane filters. But the presence of carbon residue in the ash enhances its adsorbent properties. Thus before using it to produce the ceramic products, a pre-treatment for removing carbon residue should be proceeded.

There was some relatively good agreement between chemical and phase mineral analysis. As revealed by chemical and XRD analysis, CCA was rich in potassium, calcium, and phosphorus. According to Vassilev *et al.* (2013) and references therein, significant proportions of elements such as Na, K, Ca, Mg, and P can be easily leached with water from CCA due to their occurrence in water-soluble salts (commonly chlorides, sulphates, phosphates, and carbonates). Hence, the CCA enriched with nutrient elements (mostly K, Ca, and P) has a potential to be well utilized as a soil amendment.

Additionally, CCA is satisfied with the requirement for such a material that has a high content of SiO₂, so it is possible to be used as a pozzolan in blended cement concrete to improve the compressive strength. Besides, due to the long-term strength development of CCA-blended cement concrete and the low heat of hydration recorded (Adesanya and Raheem 2010), this study also confirms the presumption that it is suitable for CCA to be used as a structural and building material. Therefore, the properties and behaviour of CCA can be more favourable for applications in mass concrete works.

Compared with the literature (Kilpimaa *et al.* 2013; Maneerung *et al.* 2016; Vassilev *et al.* 2004), it was found that the properties of CCA from gasification were typically different from those of other ashes from gasification. But from the point of utilization, there also existed some similarities between CCA from gasification and other

ashes from gasification. For example, as has been done for coal fly ash (Vassilev *et al.* 2004), the carbon residue in CCA also has a potential to be separated and to be used as activated carbon. The carbon residue in CCA can be separated by using technique of density gradient centrifugation (DGC). Details of the DGC separation procedures can be found elsewhere (Maroto-Valer *et al.* 1999). When only activation is required, high yields of activated carbon can be achieved, since the carbon residue has already undergone devolatilisation and simplification during gasification process, which is a big advantage of using carbon residue in ash from biomass gasification industries.

Furthermore, by comparing the results in this paper with other publications (Biagini *et al.* 2014; Liu *et al.* 2014; Vassilev *et al.* 2013), it can be concluded that the most notable difference between CCA from the gasification process and CCA from combustion processes is that the carbon content and specific surface area are much higher for the CCA derived from the gasification process. Pan and Eberhardt (2011) suggested that the nutrient elements in gasification ash were more bioavailable than those in combustion ash.

Finally, based on the above investigations, it becomes clear that that the main potential and sustainable utilization of the waste CCA from gasification includes mostly soil amendment and fertilization, production of construction materials and adsorbents, synthesis of minerals and production of ceramics, and recovery of valuable components. In addition, these possible applications of CCA can also provide solutions to environmental problems caused by the waste ash in biomass gasification industries.

CONCLUSIONS

1. The chemical analysis of CCA in the present study revealed that potassium and silica were the primary constituents in various crystalline forms. Being rich in potassium, calcium, and phosphorus, CCA could be regarded as a quite suitable material for soil amendment. Also, the CCA has potential to be used as a pozzolan source in blended cement concrete, since it possessed a high content of SiO₂.
2. The particle size analysis of CCA powders passed through a 0.154 mm sieve showed a mean diameter of 12.96 μm and a medium diameter of 10.23 μm. The precision of the measurements was 1.0%. The XRD data indicated the presence of crystal phases. The SEM images revealed that the ash particles were highly agglomerated, and their shapes were irregular. The EDX data indicated that the external surface of agglomerated particles was mainly coated with KCl.
3. The thermal analysis revealed that the decomposition of CCA followed a stepwise mechanism, which showed a total weight loss of 17.13 wt.% under nitrogen, that of 19.86 wt.% under air, and that of 23.12 wt.% under 40% O₂ in N₂ when the ash was being heated to 1200 °C. This result illustrated that the total weight loss increased with the rise of oxygen concentration. An endothermic peak near 620 °C in nitrogen was due to the melting of KCl, while an exothermic peak at 630 °C under oxidative atmospheres was caused by the combustion and volatilization of carbon residue.
4. The carbon content of CCA was high, which indicates, together with high porosity, that the carbon residue in the ash can potentially be separated and used as a source for

producing activated carbon. This paper provides the baseline for future work on the possible utility of the waste CCA from biomass gasification industries.

ACKNOWLEDGMENTS

The authors are grateful for the support of National Natural Science Foundation of Liaoning Province (Grant No. 2013020137) and Rural Energy Comprehensive Construction Found of the ministry of agriculture of China (Grant No. 2015-36).

REFERENCES CITED

- Abraham, R., George, J., Thomas, J., and Yusuff, K. K. M. (2013). "Physicochemical characterization and possible application of the waste biomass ash from oleoresin industries of India," *Fuel* 109, 366-372. DOI: 10.1016/j.fuel.2013.02.067
- Adesanya, D. A., and Raheem, A. A. (2010). "A study of the permeability and acid attack of corncob ash blended cements," *Construction and Building Materials* 24(3), 403-409. DOI: 10.1016/j.conbuildmat.2009.02.001
- Arvelakis, S., Jensen, P. A., and Dam-Johansen, M. (2004). "Simultaneous thermal analysis (STA) on ash from high-alkali biomass," *Energy Fuels* 18(4), 1066-1076. DOI: 10.1021/ef034065+
- Biagini, E., Barontini, F., and Tognotti, L. (2014). "Gasification of agricultural residues in a demonstrative plant: Corn cobs," *Bioresource Technology* 173(12), 110-116. DOI: 10.1016/j.biortech.2014.09.086
- Cao, Q., Xie, K. C., Bao, W. R., and Shen, S.G. (2004). "Pyrolytic behavior of waste corn cob," *Bioresource Technology* 94(1), 83-89. DOI: 10.1016/j.biortech.2003.10.031
- Du, S. L., Yang, H. P., Qian, K. Z., Wang, X. H., and Chen, H. P. (2014). "Fusion and transformation properties of the inorganic components in biomass ash," *Fuel* 117, 1281-1287. DOI: 10.1016/j.fuel.2013.07.085
- Haykiri-Acma, H., Yaman, S., and Kucukbayrak, S. (2013). "Production of biobriquettes from carbonized brown seaweed," *Fuel Processing Technology* 106(2), 33-40. DOI: 10.1016/j.fuproc.2012.06.014
- Jensen, P. A., Frandsen, F. J., Dam-Johansen, K., and Sander, B. (2000). "Experimental investigation of the transformation and release to gas phase of potassium and chlorine during straw pyrolysis," *Energy Fuels* 14(6), 1280-1285. DOI: 10.1021/ef000104v
- Kilpimaa, S., Kuokkanen, T., and Lassi, U. (2013). "Characterization and utilization potential of wood ash from combustion process and carbon residue from gasification process," *BioResources* 8(1), 1011-1027. DOI: 10.15376/biores.8.1.1011-1027
- Knudsen, J. N., Jensen, P. A., and Dam-Johansen, K. (2004). "Transformation and release to the gas phase of Cl, K, and S during combustion of annual biomass," *Energy Fuels* 18(5), 1385-1399. DOI: 10.1021/ef049944q
- Liu, X., Zhang, Y., Li, Z. F., Feng, R., and Zhang, Y. Z. (2014). "Characterization of corncob-derived biochar and pyrolysis kinetics in comparison with corn," *Bioresource Technology* 170(10), 76-82. DOI: 10.1016/j.biortech.2014.07.077
- Maneerung, T., Liew, J., Dai, Y. J., Kawi, S., Chong, C., and Wang, C. (2016). "Activated carbon derived from carbon residue from biomass gasification and its application for dye adsorption: Kinetics, isotherms and thermodynamic studies," *Bioresource*

- Technology* 200(1), 350-359. DOI: 10.1016/j.biortech.2015.10.047
- Maroto-Valer, M. M., Taulbee, and D. N., Hower, J. C. (1999). "Novel separation of the differing forms of unburned carbon present in fly ash using density gradient centrifugation," *Energy Fuels* 13(4), 947-953. DOI: 10.1021/ef990029s
- McKendry, P. (2002). "Energy production from biomass (Part 2): Conversion technologies," *Bioresource Technology* 83(1), 47-54. DOI: 10.1016/S0960-8524(01)00119-5
- Niu, Y. Q., Tan, H. Z., Wang, X. B., Liu, Z. N., Liu, H. Y., Liu, Y., and Xu, T. M. (2010). "Study on fusion characteristics of biomass ash," *Bioresource Technology* 101(23), 9373-9381. DOI: 10.1016/j.fuel.2015.06.010
- Ogundiran, M. B., Babayemi, J. O., and Nzeribe, C. G. (2011). "Determination of metal content and an assessment of the potential use of waste cashew nut ash (CNSA) as a source for potash production," *BioResources* 6(1), 529-536. DOI: 10.15376/biores.6.1.529-536
- Pan, H., and Eberhardt, T. L. (2011). "Characterization of fly ash from the gasification of wood and assessment for its application as a soil amendment," *BioResources* 6(4), 3987-4004. DOI: 10.15376/biores.6.4.3987-4004
- Park, B. D., Wi, S. G., Lee, K. H., Singh, A. P., Yoon, T. H., and Kim, Y. S. (2003). "Characterization of anatomical features and silica distribution in rice husk using microscopic and micro-analytical techniques," *Biomass Bioenergy* 25(3), 319-327. DOI: 10.1016/S0961-9534(03)00014-X
- Rajamma, R., Ball, R. J., Tarelho, L. A. C., Allen, G. C., Labrincha, J. A., and Ferreira, V. M. (2009). "Characterisation and use of biomass fly ash in cement-based materials," *Journal of Hazardous Materials* 172(2), 1049-1060. DOI: 10.1016/j.jhazmat.2009.07.109
- Terzioglu, P., and Yucel, S. (2012). "Synthesis of magnesium silicate from wheat husk ash: effects of parameters on structural and surface properties," *BioResources* 7(4), 5435-5447. DOI: 10.15376/biores.7.4.5435-5447
- Terzioglu, P., Yucel, S., Rababah, T. M., and Ozcimen, D. (2013). "Characterization of wheat hull and wheat hull ash as a potential source of SiO₂," *BioResources* 8(3), 4406-4420. DOI: 10.15376/biores.8.3.4406-4420
- Thy, P., Jenkins, B. M., Grundvig, S., Shiraki, R., and Lesher, C. E. (2006). "High temperature elemental losses and mineralogical changes in common biomass ashes," *Fuel* 85(5), 783-795. DOI: 10.1016/j.fuel.2005.08.020
- Tortosa Masiá, A. A., Buhre, B. J. P., Gupta, R. P., and Wall, T. F. (2007). "Characterising ash of biomass and waste," *Fuel Processing Technology* 88(11), 1071-1081. DOI: 10.1016/j.fuproc.2007.06.011
- Umamaheswaran, K., and Batra, V. S. (2008). "Physio-chemical characterization of India biomass ashes," *Fuel* 87(6), 628-638. DOI: 10.1016/j.fuel.2007.05.045
- Vassilev, S. V., Baxter, D., and Vassileva C. G. (2013). "An overview of the behaviour of biomass during combustion: Part I. Phase-mineral transformations of organic and inorganic matter," *Fuel* 112(10), 391-449. DOI: 10.1016/j.fuel.2013.05.043
- Vassilev, S. V., Menendez, R., Borrego, A. G., Diaz-Somoano, M., and Martinez-Tarazona, M. R. (2004). "Phase-mineral and chemical composition of coal fly ashes as a basis for their multicomponent utilization. 3. Characterization of magnetic and char concentrates," *Fuel* 83(11-12), 1563-1583. DOI: 10.1016/j.fuel.2004.01.010
- Wang, S., Jiang, X. M., Han, X. X., and Wang, H. (2008). "Fusion characteristic study on seaweed biomass ash," *Energy Fuels* 22(4), 2229-2235. DOI: 10.1021/ef800128k
- Wang, S., Zhao, X., Xing, G., and Yang, L. (2013). "Large-scale biochar production from

- crop residue: A new idea and the biogas-energy pyrolysis system,” *BioResources* 8(1), 8-11. DOI: 10.15376/biores.8.1.8-11
- Yang, H. P., Yan, R., Chen H. P., Lee, D. H., and Zheng, C. G. (2007). “Characteristics of hemicellulose, cellulose and lignin pyrolysis,” *Fuel* 86 (12), 1781-1788. DOI: 10.1016/j.fuel.2006.12.013
- Zhang, G., Reinmöller, M., Klinger, M., and Meyer, B. (2015). “Ash melting behavior and slag infiltration into alumina refractory simulating co-gasification of coal and biomass,” *Fuel* 139(1), 457-465. DOI: 10.1016/j.fuel.2014.09.029
- Zhou, W. H., Chen, G. Y., Ma, L. L., Yan, B. B., and Xia, Z. P. (2014). “Economic and environmental benefits analysis of decentralized heating using biomass gasification gas in rural area,” *Transactions of Chinese Society of Agricultural Engineering* 30(14), 213-218. DOI: 10.3969/j.issn.1002-6819.2014.14.027

Article submitted: October 19, 2015; Peer review completed: December 19, 2016;
Revised version received and accepted: February 22, 2016; Published: March 7, 2016.
DOI: 10.15376/biores.11.2.3783-3798